Path and Extent of Cross-Bridge Rotation during Muscle Contraction†

Katalin Ajtai, Daniel J. Toft, and Thomas P. Burghardt*

Department of Biochemistry and Molecular Biology, Mayo Foundation, Rochester, Minnesota 55905

Received November 24, 1993; Revised Manuscript Received February 16, 1994®

ABSTRACT: The angular distribution of myosin cross-bridges in muscle fibers was investigated in four physiological states using a multiple probe analysis of varied extrinsic probes of the cross-bridge [Burghardt & Ajtai (1994) *Biochemistry* (preceding paper in this issue)]. The analysis combines data of complementary techniques from different probes giving the highest possible angular resolution. Four extrinsic probes of the fast reactive sulfhydryl (SH1) on myosin subfragment 1 (S1) were employed. Electron paramagnetic resonance (EPR) spectra from paramagnetic probes, deuterium- and ^{15}N-substituted for greater sensitivity to orientation, on S1 were measured when the protein was freely tumbling in solution and when it was decorating muscle fibers. The EPR spectra from labeled S1 tumbling in solution were measured at X- and Q-band microwave frequencies to uniquely specify the orientation of the probe relative to the S1 principal hydrodynamic frame. The EPR spectra from labeled S1 decorating muscle fibers in rigor and in the presence of MgADP were measured at X-band and used in the multiple probe analysis of cross-bridge orientation. The time-resolved fluorescence anisotropy decay (TRFAD) of fluorescent probes on S1 was measured when the protein was freely tumbling in solution, and fluorescence polarization (FP) intensities from fluorescent probes modifying SH1 in intact muscle fibers were measured for fibers in rigor, in the presence of MgADP, in isometric contraction, and in relaxation at low ionic strength. The TRFAD measurements limit the range of possible orientations of the probe relative to the S1 principal hydrodynamic frame. The FP intensity measurements were used in the multiple probe analysis of cross-bridge orientation. The combination of the EPR and FP data determined a highly resolved cross-bridge angular distribution in rigor, in the presence of MgADP, in isometric contraction, and in relaxation at low ionic strength. These findings confirm earlier observations of a rigid body rotation of the SH1 region in the myosin head group upon physiological state changes and indicate the path and extent of cross-bridge rotation during contraction. The rotation of the cross-bridge is visualized with computer-generated space-filling models of actomysin in six states of the contraction cycle.

Certain well-known models of force production in muscle fibers and many experimental observations implicate the rotation of the myosin cross-bridge in the production of force (Huxley, 1969; Huxley & Simmons, 1971; Borejdo et al., 1979; Irving et al., 1992). Spectroscopic probe studies of cross-bridge orientation, employing electron paramagnetic resonance (EPR) and fluorescence polarization (FP), contributed to the experimental findings by both supporting (Burghardt et al., 1983) and contradicting (Cooke et al., 1982) the rotating cross-bridge model. These contradictions raised the question of whether or not extrinsic probes report local or global changes in cross-bridge attitude (Tanner et al., 1992). We show that, by properly using well-established protocols to label cross-bridges and to verify stability and specificity of the probe, the probes we use to report cross-bridge rotation reflect a global change in cross-bridge attitude (Ajtai et al., 1992a). Therefore, the rationalization of the conflicting probe data necessitated the development of our multiple probe analysis (MPA) method capable of accounting for probe data from various experimental methods and probes (Burghardt & Ajtai, 1992). We demonstrated the applicability of the MPA for detecting cross-bridge orientation in labeled muscle fibers (Ajtai et al., 1992b). Improvements to the MPA method described here and in the accompanying paper permit a more refined view of the angular disposition of the cross-bridge in an extended set of physiological states including the active isometric state.

The combination of data from complementary techniques is the basis for the refinement in the probe angular distribution, in the MPA method, over single probe methods. We showed that, by combining data from EPR spectra and FP intensities of labeled muscle fibers, we produced a well-defined representation of the angular distributions of the individual probes in two physiological states (Ajtai et al., 1992b). Still further improvement is possible by (i) making use of data from the isolated myosin subfragment 1 (S1) tumbling freely in solution and (ii) using a larger and more general set of FP intensities from the labeled fiber.

From solution studies with EPR and time-resolved anisotropy decay (TRFAD), we estimate the relationship between the probe fixed coordinate frame and the principal hydrodynamic frame of S1 (the probe fixed coordinate frame is either the principal magnetic frame of the spin probe or the transition dipole frame of the fluorescent probe). The relationship between the probe and protein coordinate frames and the protein rotational diffusion constants determines the shape of the EPR spectrum from freely tumbling S1 (Freed, 1976). At X-band microwave frequency EPR simulations indicated no unique solution for the probe–protein relationship, but the combination of X- and Q-band simulations indicated a unique solution. TRFAD measurement of the probe–protein relationship is more ambiguous but nonetheless constrains the parameters used in the MPA method. With this information, the MPA of data from muscle fibers estimates the high-resolution angular distribution of the principal hydrodynamic frame of the myosin cross-bridge.

† This work was supported by the National Institutes of Health (R01 AR 39288), the American Heart Association (Grant-in-Aid 930 06610), and the Mayo Foundation.

* Address correspondence to this author.

® Abstract published in *Advance ACS Abstracts,* April 1, 1994.

0006-2960/94/0433-5382$04.50/0

We showed that a feature of the MPA could make use of a larger set of FP intensities to estimate odd-rank order parameters of an angular distribution (Burghardt & Ajtai, 1992). We develop this idea here and apply it to labeled muscle fibers to estimate odd-rank order parameters for the angular distribution of the cross-bridge. These order parameters eliminate all of the fundamental ambiguities in our determination of the cross-bridge angular distribution.

We find that the cross-bridge angular distribution changes dramatically as a function of the fiber physiological state. If we approximate the shape of the S1 with a prolate ellipsoid and designate a polar or torsional rotation as one in which the long or short axis of the S1 is rotated, respectively, then force generation involves predominantly polar rotations with amplitudes averaging 35–45°. State transitions in the cross-bridge cycle related to the ATPase activity, such as binding or releasing of nucleotides (the transitions from rigor to low ionic strength relaxed or from the MgADP state to rigor), involve predominantly torsional rotations with amplitudes averaging 5–10°. The separation of the cross-bridge function into different modes of rotation suggests that the enzymatic events, known to modulate the actomyosin affinity, involve torsional motion for the favorable alignment of complementary sites on myosin and actin at the actomyosin interface. The subsequent strong interaction causes polar rotation and consequently force development.

MATERIALS AND METHODS

Chemicals. The spin label [^{15}N,^{2}H]-*N*-(1-oxy-2,2,6,6-tetramethyl-4-piperidinyl)maleimide ([^{15}N,^{2}H]MTSL) was a generous gift from Dr. Albert Beth (Department of Molecular Physiology and Biophysics, Vanderbilt University, Nashville, TN 37232). The spin label 3-(2′-iodoacetamido)-2,2,5,5-tetramethylpyrrolidine-d_{15}-*1*-^{15}*N*-1-oxyl ([^{15}N,^{2}H]-IPSL) was custom made by MSD Isotopes (Montreal, Canada). The fluorescent labels *N*-[[(iodoacetyl)amino]-ethyl]-5-naphthylamine-1-sulfonic acid (1SIA) and 5′-(iodoacetamido)tetramethylrhodamine (5′IATR) were from Molecular Probes (Eugene, OR). ADP, ATP, DTT, P^1,P^5-di(adenosine 5′) pentaphosphate (Ap_5A), phenylmethanesulfonyl fluoride (PMSF), glucose, hexokinase, phosphocreatine, and creatine kinase are from Sigma (St. Louis, MO). Ammonium sulfate (ultrapure) is from Schwarz/Mann Biotechnology (Cleveland, OH). All chemicals are of analytical grade.

Solutions. Rigor solution is 80 mM potassium chloride, 5 mM magnesium chloride, 2 mM ethylene glycol bis(β-aminoethyl ether)-*N*,*N*,*N*′,*N*′-tetraacetic acid (EGTA), and 5 mM phosphate buffer at pH 7.0. Relaxing solution is rigor solution with 4 mM ATP added. MgADP solution is rigor solution with 4 mM ADP, 100 μM diadenosine pentaphosphate (Ap_5A) to inhibit myofibrillar myokinase from converting ADP to ATP, and an ADP-regenerating system of 10 mM glucose and 0.1 mg/mL hexokinase to convert ATP to ADP. Low ionic strength relaxing solution is similar to that described by Brenner et al. (1982) with 1 mM Na_2ATP, 1 mM EGTA, 3 mM $MgCl_2$, and 5 mM phosphate buffer at pH 7.0. We calculated that this solution has an ionic strength of 25 mM. Activating solution is relaxing solution with 0.1 mM $CaCl_2$ replacing EGTA, 4 mM phosphocreatine, and 0.4 mg/mL creatine kinase to generate ATP. All of the buffers for fluorescent measurements also contain 1 mM DTT.

Preparation of Labeled Myosin Subfragment 1. Rabbit myosin was prepared by a standard method (Tonomura et al., 1966). We used α-chymotrypsin to digest myosin filaments in the preparation of myosin S1 (Weeds & Taylor, 1975). The specific labeling of SH1 on S1 with [^{15}N,^{2}H]MTSL ([^{15}N,^{2}H]MTSL-S1) and [^{15}N,^{2}H]IPSL ([^{15}N,^{2}H]IPSL-S1) is identical to that for the unsubstituted probes MTSL and IPSL, respectively, including the treatment with potassium ferricyanide to selectively destroy radials not linked to SH1 (Graceffa & Seidel, 1980; Ajtai et al., 1990). The preparation of the ammonium sulfate precipitated spin-labeled proteins is also identical to that for the unsubstituted spin-labeled protein preparation (Ajtai et al., 1990).

The specific labeling of SH1 on S1 with 1SIA (1SIA-S1) was carried out as described by Duke et al. (1976). The specific labeling of SH1 with 5′IATR (5′IATR-S1) was carried out as described by Ajtai et al. (1992a) with a labeling solution containing a molar ratio of dye:protein of 1:1.

Specificity of Protein-Bound Labels. We measured the extent of probe labeling of the SH1's using K^+-EDTA and Ca^{2+}-ATPase activities of labeled S1. The specificity of [^{15}N,^{2}H]MTSL, 1SIA, and 5′IATR for SH1 for these labeling conditions was identical to that described previously (Ajtai et al., 1992a,b). The specificity of [^{15}N,^{2}H]IPSL-modified S1 behaved in a manner identical to that observed previously for the unsubstituted probe (Ajtai et al., 1990). The spin-labeled S1 ATPase indicates specific and efficient (0.6–0.7 mol of spin/mol of S1) modification of the SH1 group.

Muscle Fibers. Rabbit psoas muscle fibers were obtained as previously described (Borejdo et al., 1979) and kept in a relaxing solution containing 50% glycerol (volume to volume) at −15 °C for up to several weeks. In EPR experiments fiber bundles of ~50 glycerinated fibers each were washed for 30 min in relaxing solution, to remove the glycerol, and then transferred to skinning solution for 30 min, to remove cell members that my inhibit diffusion of S1 through the fiber bundles. The fibers were then thoroughy washed first in relaxing solution (15 min) and then in rigor solution (20 min). These fibers bundles were incubated in rigor buffer containing spin-labeled S1 at a concentration of 4–6 mg/mL for 6–14 h in the dark at 4 °C. PMSF was added at 100 μM concentration to the rigor solution during incubation of the fibers with spin-labeled S1 to inhibit tissue proteases from digesting the fiber. The labeled fiber bundles were washed in rigor for ~30 min to remove the unbound S1 and then incubated in either rigor or ADP solution for 30 min. The fibers were then cut to uniform lengths of ~4 mm and arranged with parallel fiber axes in a quartz flat tissue cell (Wilmad Glass, Buena, NJ) for the EPR studies.

We estimated the contribution of the free S1 to the decorated fiber EPR spectrum by comparing it to the EPR spectrum from the labeled S1 in solution. The spectrum from a decorated fiber with the fiber axis parallel to the Zeeman field shows a very slight contribution from the high-field resonance, characteristic of free labeled S1. We estimate the contamination of free labeled S1 to the decorated fiber spectrum to be <5%.

We prepared 1SIA- and 5′IATR-labeled glycerinated muscle fibers using the procedure of Borejdo and Putnam (1977) and Ajtai et al. (1992a), respectively. These earlier publications indicated that 86% of the 1SIA and 77% of the 5′IATR are localized on the heavy chain of myosin with the remainder on actin, α-actinin, tropomyosin, and light chain 1 (LC1). The myosin ATPase from myosin extracted from the labeled fibers indicates that all of the dye on the heavy chain resides on SH1 (Ajtai & Burghardt, 1989). Modification of SH1 with 1SIA or 5′IATR does not impair fiber contractility even when the degree of labeling is as high as 0.4

mol of fluorophore/mol of S1 (Nihei et al., 1974; Burghardt et al., 1984).

EPR Measurements. EPR spectra were measured at X-band on a Bruker Model ER300 (Bruker Instruments, Bilerica, MA) with a TM_{110} cylindrical cavity. The Q-band measurements were carried out on a Bruker Model ER300e with a TE_{011} cavity. All EPR spectra were measured at 5 °C.

The EPR spectrum is sensitive to changes in the spin probe orientation through the resonance Zeeman field value and the transition probability. We find that the EPR spectrum is sensitive to only two of three angular degrees of freedom of the probe, the probe polar and torsional angles measured relative to the principal magnetic frame (Ajtai et al., 1992b).

Fluorescence Measurements. Steady-state measurements were carried out on a SLM 8000 fluorescence spectrophotometer (SLM Instruments, Urbana, IL) in L-format and TRFAD measurements on a time-domain instrument described previously (Ajtai et al., 1992a). All measurements were conducted at 5 °C. Experiments on 1SIA-labeled fibers used an excitation wavelength of $\lambda_{ex} = 330 \pm 4$ or 410 ± 4 nm and an emission wavelength of $\lambda_{em} = 500 \pm 20$ nm. Experiments on 5'IATR-labeled fibers used $\lambda_{ex} = 550 \pm 2$ nm and $\lambda_{em} = 600 \pm 20$ nm.

An experiment on a fluorescent-labeled muscle fiber consisted of measuring a matrix of fluorescence intensities, $F(\psi,\chi,\lambda_{ex},\lambda_{em})$, corresponding to ψ, χ = 0, 30°, 54.7°, and 90° (16 intensities), where ψ is the excitation and χ the emission polarization measured relative to the fiber axis, as described previously (Ajtai et al., 1992b). The intensities are combined into the 15 ratios, R_i, of the form

$$R_1 \equiv \frac{F(1,1) - F(1,4)}{F(1,1) + F(1,4)}, \quad R_2 \equiv \frac{F(4,4) - F(4,1)}{F(4,4) + F(4,1)}, \quad R_3 \equiv \frac{F(1,1) - F(4,1)}{F(1,1) + F(4,1)} \tag{1}$$

$$R_4 \equiv \frac{F(2,2) - F(2,3)}{F(2,2) + F(2,3)}, \quad R_5 \equiv \frac{F(3,3) - F(3,2)}{F(3,3) + F(3,2)}, \quad R_6 \equiv \frac{F(2,2) - F(3,2)}{F(2,2) + F(3,2)} \tag{2}$$

$$R_7 \equiv \frac{F(1,2) - F(1,3)}{F(1,2) + F(1,3)}, \quad R_8 \equiv \frac{F(2,1) - F(3,1)}{F(2,1) + F(3,1)}, \quad R_9 \equiv \frac{F(1,2) - F(3,1)}{F(1,2) + F(3,1)} \tag{3}$$

$$R_{10} \equiv \frac{F(4,2) - F(4,3)}{F(4,2) + F(4,3)}, \quad R_{11} \equiv \frac{F(2,4) - F(3,4)}{F(2,4) + F(3,4)}, \quad R_{12} \equiv \frac{F(4,2) - F(3,4)}{F(4,2) + F(3,4)} \tag{4}$$

$$R_{13} \equiv \frac{F(1,1) - F(3,3)}{F(1,1) + F(3,3)}, \quad R_{14} \equiv \frac{F(2,2) - F(2,1)}{F(2,2) + F(2,1)}, \quad R_{15} \equiv \frac{F(1,2) - F(2,4)}{F(1,2) + F(2,4)} \tag{5}$$

where the parameters λ_{ex} and λ_{em} are suppressed from the argument of F and indexes 1, 2, 3, and 4 are the shorthand notation for 0, 30°, 54.7°, and 90°, respectively. The subsets of ratios R_i with i = 1, 2, 3 are the polarization ratios usually denoted as $P_\parallel$, $P_\perp$, and $Q_\parallel$. The definition of the set of 15 ratios is somewhat arbitrary. These were selected because they incorporated the traditional ratios and because they were the minimum number that gave satisfactory results. Any choice must include intensities for which ψ and χ are not equal to 0 and 90°; otherwise, the ratios will not be influenced by the odd-rank order parameters.

Protein Angular Distribution. The cross-bridge angular distribution function N describes the orientation of the principal hydrodynamic frame relative to the laboratory frame. Expanding N in a set of complete orthonormal angular functions, $D^j_{m,n}$, with order parameter coefficients, we have

$$N(\alpha,\beta,\gamma) = \sum_{j=0}^{\infty} \sum_{m,n=-j}^{j} a^j_{m,n}((2j+1)/8\pi^2)^{1/2} D^j_{m,n}(\alpha,\beta,\gamma) \tag{6}$$

where Euler angles α and β are the protein azimuth and polar angles relative to the fiber axis of symmetry and γ is the torsion angle. Coefficients $a^j_{m,n}$ are order parameters of rank j.

Assuming that the laboratory z-axis is parallel to the fiber axis and that the fiber axis is a symmetry axis (Burghardt et al., 1983), then

$$a^j_{m,n} = a^j_{0,n}\delta_{m,0} \tag{7}$$

where $\delta_{i,j}$ is the Kronecker delta. A protein angular distribution obtained from the MPA program uses eqs 6 and 7 to give

$$N(\beta,\gamma) = \sum_{j=0}^{6} \sum_{n=-j}^{j} a^j_{0,n}((2j+1)/8\pi^2)^{1/2} D^j_{0,n}(\beta,\gamma) \tag{8}$$

where the sum in j includes the odd-rank order parameters except j = 5. We make use of two special cases of eq 8 to emphasize features belonging to the two degrees of rotational freedom of the cross-bridge in a fiber. The torsinal angular distribution, $m(\gamma)$, is obtained from $N(\beta,\gamma)$ by summing over β such that

$$m(\gamma) = \int_0^{\pi} N(\beta,\gamma) \sin\beta \, d\beta \tag{9}$$

The polar angular distribution function, $n(\beta)$, is obtained from $N(\beta,\gamma)$ by summing over γ such that

$$n(\beta) = \int_0^{2\pi} N(\beta,\gamma) \, d\gamma \tag{10}$$

RESULTS

(A) EPR Spectra of Immobilized Spin-Labeled S1. The X- and Q-band spectra of immobilized [^{15}N,^{2}H]MTSL-S1 and [^{15}N,^{2}H]IPSL-S1 and their best fits are shown in Figure 1. We fitted these spectra using the methods described in the accompanying paper. The X- and Q-band spectra for each probe were fitted simultaneously to determine their common spectral parameters. The spectra from [^{15}N,^{2}H]MTSL-S1 were best fitted by a random distribution of probes with a Gaussian line shape and the spectral parameters $g_x = 2.0087 \pm 0.0001$, $g_y = 2.0058 \pm 0.0001$, $g_z = 2.0021 \pm 0.0001$, $T_x = 10.7 \pm 0.1$ G, $T_y = 10.5 \pm 0.1$ G, $T_z = 49.8 \pm 0.1$ G, $\epsilon_{m=-1/2} = 1.2 \pm 0.1$ G, and $\epsilon_{m=1/2} = 1.3 \pm 0.1$ G and a post-line-shape calculation Gaussian broadening of 0.5 G, with $\hbar\omega/(\beta_e g_e) = 3509.3$ G for X-band and 12134.6 G for Q-band, where $2\pi\hbar$ is Planck's constant, ω is the microwave frequency, β_e is the Borh magneton, and g_e is the g-factor for a free electron. The value of $\hbar\omega/(\beta_e g_e)$ was found by allowing it to freely vary for the best fit.

The spectra from [^{15}N,^{2}H]IPSL-S1 were best fitted by a random distribution of probes with a Lorentzian line shape and the spectral parameters $g_x = 2.0092 \pm 0.0001$, $g_y = 2.0070 \pm 0.0001$, $g_z = 2.0036 \pm 0.0001$, $T_x = 9.2 \pm 0.1$ G, $T_y = 9.2$

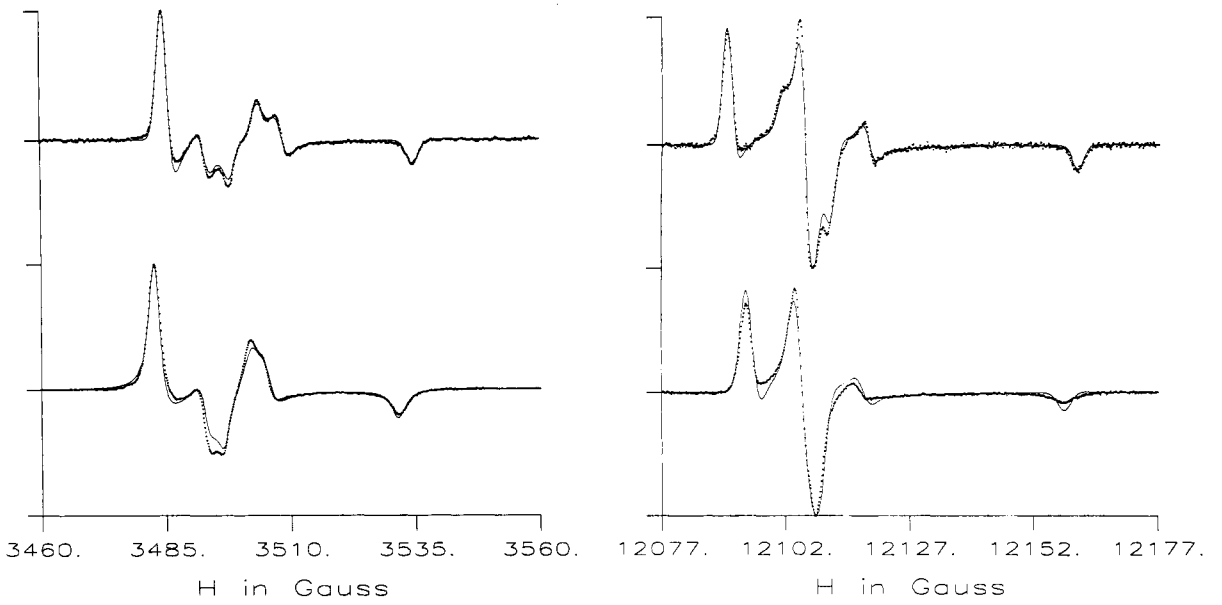

FIGURE 1: X-band (left) and Q-band (right) EPR spectrum from [^{15}N,^{2}H]MTSL-S1 (top) and [^{15}N,^{2}H]-IPSL-S1 (bottom) precipitated in ammonium sulfate (dots) and the best fit (solid line).

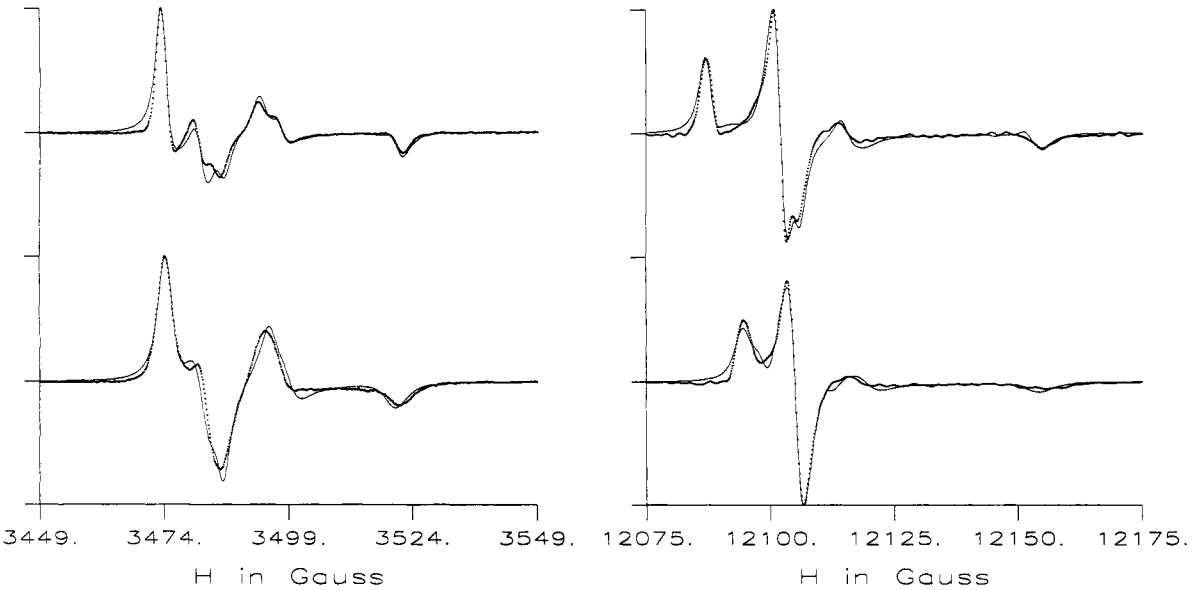

FIGURE 2: X-band (left) and Q-band (right) EPR spectrum from [^{15}N,^{2}H]MTSL-S1 (top) and [^{15}N,^{2}H]IPSL-S1 (bottom) freely tumbling in rigor buffer (dots) and the best fit (solid line).

± 0.1 G, T_z = 48.7 ± 0.1 G, $\epsilon_{m=-1/2}$ = 1.3 ± 0.1 G, and $\epsilon_{m=1/2}$ = 1.6 ± 0.1 G and a post-line-shape calculation Gaussian broadening of 0.5 G, with $\hbar\omega/(\beta_e g_e)$ = 3524.5 G for X-band and 12149.3 G for Q-band. The value of $\hbar\omega/(\beta_e g_e)$ was found by allowing it to freely vary for the best fit.

(B) EPR Spectra of Spin-Labeled S1 Freely Tumbling in Solution. The X- and Q-band spectra of freely rotationally diffusing [^{15}N,^{2}H]MTSL-S1 and [^{15}N,^{2}H]IPSL-S1 and their best fits are shown in Figure 2. We fitted these spectra using the methods described in the accompanying paper with spectral parameters determined from the immobilized samples held fixed and assuming that S1 is an ellipsoid of revolution. The adjustable parameters were the rotational diffusion constants of S1, $D_1 = D_2, D_3$; the Euler angles relating the probe magnetic frame with the principal hydrodynamic frame of S1, $\Omega_{i\rightarrow j}$ (see Figure 2 in accompanying paper); the spectral width, ϵ_m; and the cone angle for local probe movement, ζ.

The X- and Q-band spectra for individual probes were fitted simultaneously while $\Omega_{i\rightarrow j}$, ϵ_m, and ζ were varied. The X- and Q-band spectra for both probes were fitted simultaneously while D_1 and D_3 were varied. We find that $D_1 = D_2$ = (2.2 ± 1.0) × 10^5 s^{-1} and D_3 = (10.0 ± 2.0) × 10^5 s^{-1}. Furthermore, if $\Omega_{i\rightarrow j} = (\alpha_{i\rightarrow j}, \beta_{i\rightarrow j}, \gamma_{i\rightarrow j})$, then for [^{15}N,^{2}H]MTSL-S1, $\Omega_{1\rightarrow 9}$ = (60 ± 2°, 20 ± 2°, –) or (240 ± 2°, 160 ± 2°, –) and ζ = 9 ± 1°, and for [^{15}N,^{2}H]IPSL-S1, $\Omega_{2\rightarrow 9}$ = (50 ± 2°, 90 ± 2°, –) or (230 ± 2°, 90 ± 2°, –) and ζ = 10 ± 1°. Angle $\gamma_{i\rightarrow j}$ is arbitrary, and both probes have the two equivalent choices indicated for the other Euler angles in the fit of these EPR spectra because S1 is an ellipsoid of revolution. The spectral widths did not change from those values observed from the immobilized spectra and reported in section A above. The rotational diffusion constants are related to the ratio $p = a/b$, where $a(b)$ is the major (minor) axis length in the prolate ellipsoid assumed for the shape of S1 (Cantor & Schimmel, 1980). We find that p = 3.8 for S1. This is a 10% more elongated shape than that suggested by Mendelson et al. (1973).

We recorded the X- and Q-band spectra of freely rotationally diffusing [^{15}N,^{2}H]MTSL-S1 and [^{15}N,^{2}H]IPSL-S1 in the presence of nucleotide (MgATP and MgADP; data not shown). The spectrum of [^{15}N,^{2}H]MTSL-S1 in the presence of nucleotide is identical to that for rigor at both frequencies, as

FIGURE 3: X-band EPR spectrum of [^{15}N,^{2}H]IPSL-S1 decorating muscle fibers in rigor (left) and in the presence of MgADP (right) for fibers parallel (top) and perpendicular (bottom) to the fiber axis. The dotted line is the data, and the solid line is the best fit.

observed previously at X-band (Ajtai et al., 1992b). The spectrum of [^{15}N,^{2}H]IPSL-S1 in the presence of nucleotide is slightly different from that for rigor, also as observed previously at X-band with the unsubstituted probe (Ajtai et al., 1990). We modeled the potential effect of nucleotide on the probe in [^{15}N,^{2}H]IPSL-S1 by fitting the EPR spectra in the presence of nucleotide, using the same parameter values found in the absence of nucleotide except that we allowed the spectral width and cone angle to vary in search of the best fit. We found that the best fit in the presence of nucleotide had identical spectral widths to within ±0.05 G and an identical cone angle to within ±1°. We concluded that nucleotide binding does not significantly mobilize the spin label.

(C) EPR Spectra of Spin-Labeled S1 Decorating Muscle Fibers. The spectra of [^{15}N,^{2}H]MTSL-S1 decorating muscle fibers in rigor and in the presence of MgADP were published (Ajtai et al., 1992b). The spectra of [^{15}N,^{2}H]IPSL-S1 decorating muscle fibers in these conditions and their best fits are shown in Figure 3. We fitted these spectra using the methods described in the accompanying paper with spectral parameters determined from the immobilized samples except that the spectral width and cone angle values were taken from the freely tumbling S1 samples. The only adjustable parameter was $\hbar\omega/(\beta_e g_e)$. These data were used to constrain the order parameters of the cross-bridge orientation distribution for fibers in rigor and in the presence of MgADP in the MPA.

(D) Fluorescence Polarization Spectra of Immobilized Fluorescent-Labeled S1. The fluorescence polarization from immobilized labeled S1 indicates the angle, θ, between the absorption and emission dipoles. These spectra were published previously and indicate that for 15IA with λ_{em} = 500 nm and λ_{ex} = 330 or 410 nm, $\theta(1\text{5IA})_{330}$ = 40.9° or $\theta(1\text{5IA})_{410}$ = 22.3° (Ajtai et al., 1992b). For 5′IATR with λ_{em} = 600 nm and λ_{ex} = 550 nm, $\theta(5'\text{IATR})_{550}$ = 18.7° (Ajtai et al., 1992a).

(E) Time-Resolved Fluorescence Anisotropy Decay (TRFAD) from Labeled S1 Freely Tumbling in Solution. TRFAD measurements from 1 5IA-labeled S1 freely tumbling in solution were performed with λ_{em} = 500 nm and λ_{ex} = 330 or 360 nm (λ_{ex} = 410 nm was not available from the laser-based system). We found, as shown previously (Mendelson et al., 1973), that the anisotropy relaxation is dominated by a single exponential relaxation (data not shown), indicating that the transition dipoles are roughly aligned with the major axis of the principal hydrodynamic frame of S1. This is true in the presence and absence of nucleotide. This restriction is used to constrain the Euler angles, $\Omega_{13\to0}$ (see Figure 2 in the accompanying paper), by requiring that the angle between either transition dipole and the major axis of the principal hydrodynamic frame be ≤40°.

The cone angle for independent probe movement, ζ, is also indicated by the TRFAD curve (Lakowicz, 1983). In agreement with previous studies our data indicated $\zeta < 2°$ or nearly no independent probe movement for 1 5IA in the presence and absence of nucleotide (Mendelson et al., 1975). The TRFAD curve for 5′IATR-S1 is not sensitive to the slow rotational motion of S1 because the fluorescence lifetime of 5′IATR is short (~4 ns compared with the S1 rotational relaxation time of ~70–200 ns; Ajtai et al., 1992a). TRFAD offers no constraining information concerning the orientation of 5′IATR on S1. On the question of the independent movement of 5′IATR on S1, we showed previously that the TRFAD curve suggests that ζ = 10° in the presence and absence of nucleotide (Ajtai et al., 1992a).

(F) Steady-State Fluorescence Polarization from Labeled Muscle Fibers in Rigor, MgADP, Isometric Contraction, and Relaxation at Low Ionic Strength. The fluorescence polarization excitation spectra for 1 5IA- and 5′IATR-labeled fibers in rigor, in the presence of MgADP, in relaxation, and in active isometric contraction were published (Ajtai et al., 1992a,b). These data indicate a distinctive distribution of probes for each physiological state of the fiber. We reinvestigated this system to supply to extended data set required for the multiple probe analysis and to investigate the low ionic strength relaxed condition. We measured the 15 FP ratios indicated in eqs 1–5 for 1 5IA-(5′IATR-) labeled fibers at two (one) excitation wavelengths and four physiological states. These data are summarized in Table 1.

In relaxation at low ionic strength ~50% of the cross-bridges at any instant are actin bound (Brenner et al., 1982; Brenner, 1990). In our analysis we assume that the detached cross-bridges are randomly distributed. This assumption is not rigorously correct since it is known that detached cross-bridges have low but detectable order (Burghardt et al., 1984). To improve on this treatment, we would include the relaxed state as the fifth physiological state in the MPA of cross-bridge order and orientation. This complication, however, expands the computing requirements of the problem beyond our present capability and was not attempted.

Table 1: Fluorescence Polarization Ratios[a]

		rigor	MgADP	active	LI relax
R_1	(a)	0.303 ± 0.006	0.343 ± 0.005	0.300 ± 0.005	0.308 ± 0.007
	(b)	0.395 ± 0.007	0.440 ± 0.006	0.417 ± 0.006	0.443 ± 0.009
	(c)	0.328 ± 0.010	0.594 ± 0.004	0.517 ± 0.005	0.496 ± 0.017
R_2	(a)	−0.241 ± 0.006	−0.278 ± 0.006	−0.168 ± 0.005	−0.173 ± 0.007
	(b)	−0.221 ± 0.005	−0.226 ± 0.007	−0.137 ± 0.006	−0.157 ± 0.009
	(c)	0.167 ± 0.007	−0.288 ± 0.006	−0.166 ± 0.006	−0.193 ± 0.021
R_3	(a)	0.198 ± 0.008	0.203 ± 0.008	0.180 ± 0.009	0.194 ± 0.011
	(b)	0.192 ± 0.009	0.235 ± 0.008	0.361 ± 0.009	0.394 ± 0.012
	(c)	0.308 ± 0.013	0.543 ± 0.021	0.468 ± 0.011	0.449 ± 0.012
R_4	(a)	0.096 ± 0.003	0.112 ± 0.004	0.092 ± 0.003	0.100 ± 0.005
	(b)	0.120 ± 0.003	0.134 ± 0.003	0.122 ± 0.003	0.136 ± 0.005
	(c)	0.066 ± 0.005	0.196 ± 0.002	0.158 ± 0.004	0.156 ± 0.010
R_5	(a)	−0.090 ± 0.003	−0.106 ± 0.004	−0.076 ± 0.003	−0.086 ± 0.005
	(b)	−0.100 ± 0.003	−0.109 ± 0.003	−0.089 ± 0.003	−0.106 ± 0.005
	(c)	−0.006 ± 0.004	−0.163 ± 0.002	−0.118 ± 0.003	−0.117 ± 0.010
R_6	(a)	0.062 ± 0.003	0.061 ± 0.004	0.048 ± 0.005	0.052 ± 0.005
	(b)	0.111 ± 0.012	0.111 ± 0.010	0.101 ± 0.004	0.115 ± 0.005
	(c)	0.080 ± 0.008	0.249 ± 0.018	0.155 ± 0.005	0.136 ± 0.007
R_7	(a)	0.102 ± 0.003	0.119 ± 0.004	0.101 ± 0.003	0.110 ± 0.005
	(b)	0.136 ± 0.003	0.151 ± 0.003	0.145 ± 0.003	0.154 ± 0.005
	(c)	0.117 ± 0.003	0.214 ± 0.003	0.186 ± 0.003	0.180 ± 0.008
R_8	(a)	0.069 ± 0.003	0.068 ± 0.004	0.061 ± 0.004	0.066 ± 0.005
	(b)	0.126 ± 0.012	0.130 ± 0.009	0.124 ± 0.003	0.134 ± 0.005
	(c)	0.132 ± 0.007	0.265 ± 0.019	0.178 ± 0.005	0.158 ± 0.007
R_9	(a)	0.009 ± 0.005	0.000 ± 0.005	0.003 ± 0.008	0.016 ± 0.010
	(b)	0.007 ± 0.013	0.006 ± 0.011	0.081 ± 0.008	0.116 ± 0.009
	(c)	0.120 ± 0.008	0.254 ± 0.024	0.154 ± 0.007	0.118 ± 0.018
R_{10}	(a)	0.078 ± 0.002	0.095 ± 0.004	0.053 ± 0.003	0.066 ± 0.005
	(b)	0.072 ± 0.003	0.075 ± 0.003	0.044 ± 0.002	0.059 ± 0.004
	(c)	−0.054 ± 0.003	0.104 ± 0.002	0.058 ± 0.002	0.066 ± 0.008
R_{11}	(a)	0.046 ± 0.004	0.045 ± 0.004	0.015 ± 0.004	0.017 ± 0.005
	(b)	0.067 ± 0.011	0.054 ± 0.011	0.027 ± 0.004	0.040 ± 0.004
	(c)	−0.039 ± 0.008	0.154 ± 0.019	0.051 ± 0.006	0.048 ± 0.008
R_{12}	(a)	0.103 ± 0.007	0.130 ± 0.008	0.092 ± 0.008	0.091 ± 0.008
	(b)	0.176 ± 0.011	0.168 ± 0.012	0.056 ± 0.010	0.071 ± 0.008
	(c)	−0.019 ± 0.008	0.196 ± 0.023	0.080 ± 0.011	0.074 ± 0.017
R_{13}	(a)	0.285 ± 0.007	0.313 ± 0.008	0.243 ± 0.009	0.272 ± 0.008
	(b)	0.329 ± 0.007	0.359 ± 0.006	0.374 ± 0.005	0.390 ± 0.015
	(c)	0.220 ± 0.014	0.601 ± 0.016	0.471 ± 0.008	0.453 ± 0.019
R_{14}	(a)	−0.099 ± 0.004	−0.110 ± 0.003	−0.087 ± 0.005	−0.091 ± 0.005
	(b)	−0.119 ± 0.005	−0.132 ± 0.003	−0.114 ± 0.005	−0.098 ± 0.009
	(c)	−0.055 ± 0.005	−0.138 ± 0.004	−0.123 ± 0.003	−0.129 ± 0.010
R_{15}	(a)	0.235 ± 0.008	0.267 ± 0.007	0.218 ± 0.007	0.232 ± 0.007
	(b)	0.250 ± 0.012	0.287 ± 0.009	0.318 ± 0.012	0.366 ± 0.009
	(c)	0.174 ± 0.011	0.533 ± 0.009	0.426 ± 0.008	0.402 ± 0.017

[a] Fluorescence polarization ratios for muscle fibers in rigor, in the presence of MgADP, in isometric contraction, and in relaxation at low ionic strength labeled with (a) 15IA with λ_{ex} = 330 nm and λ_{em} = 500 nm, (b) 15IA with λ_{ex} = 410 nm and λ_{em} = 500 nm, and (c) 5′IATR with λ_{ex} = 550 nm and λ_{em} = 600 nm.

Table 2: Euler Angles (deg)[a]

rotation	α	β	γ	rotation	α	β	γ
(1) $\Omega_{1\to9}$	60	20	240	(7) $\Omega_{9\to11}$	0	35	0
	240	160	120		180	35	180
(2) $\Omega_{2\to9}$	50	90	0	(8) $\Omega_{9\to12}$	175	10	190
	50	90	0		5	10	350
(3) $\Omega_{3\to9}$	180	40	120	(9) $\Omega_{10\to9}$	−10	0	0
	0	40	60		10	0	0
(4) $\Omega_{4\to9}$	200	40	120	(10) $\Omega_{11\to10}$	180	35	−170
	340	40	60		−10	35	0
(5) $\Omega_{5\to9}$	190	60	300	(11) $\Omega_{0\to9}$	0	87	140
	190	120	60		0	87	40
(6) $\Omega_{9\to10}$	10	0	0				
	350	0	0				

[a] Euler angles 1–5 relate the probe frame with the principal hydrodynamic frame of myosin S1. Euler angles 6–10 relate the principal hydrodynamic frame of S1 in four physiological states of the fiber. Euler angles $\Omega_{0\to9}$ relate the laboratory frame with the principal hydrodynamic frame of S1 in a fiber in rigor. The top (bottom) row of Euler angles for each rotation corresponds to the two equivalent solutions, A and B, as discussed in section H of Results. All angles are ±5°.

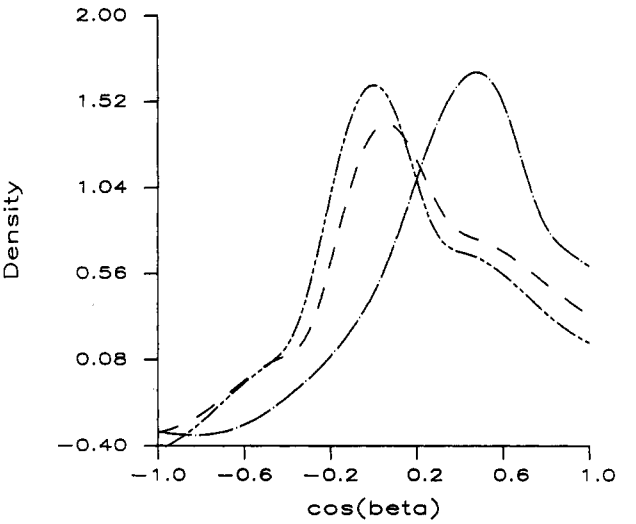

FIGURE 4: Polar angular distribution, $n(\beta)$, for muscle fiber cross-bridges in rigor (- - -), isometric contraction (— · —), and low ionic strength relaxing condition (— - - —).

(*G*) *Euler Angles.* We combined data sets using the MPA from [^{15}N,^{2}H]MTSL-S1 and [^{15}N,^{2}H]IPSL-S1 decorating fibers in rigor and in the presence of MgADP with the 15 FP ratios from 15IA- and 5′IATR-labeled fibers in rigor, MgADP, isometric contraction, and relaxation at low ionic strength. The data from 15IA included two excitation wavelengths. The solution yields the Euler angles and order parameters for the states. We find that two different solutions equivalently satisfy the imposed constraints. Both solutions give the most likely orientation of the major axis of the rigor cross-bridge to be 87° from the fiber axis. The Euler angles of these solutions, designated solutions A and B, are given in Table 2. Table 2 also indicates the most likely Euler angles relating the laboratory fixed frame with the principal hydrodynamic frame of a cross-bridge in rigor, $\Omega_{0\to9}$. Angles $\Omega_{0\to9}$ were determined by maximizing the overlap of the angular distributions of the principal hydrodynamic and probe reference frames with the laboratory frame coordinate axes appropriately rotated by the other Euler angles in Table 2.

The Euler angles of the state transitions related to the binding of nucleotide, $\Omega_{9\to12}$, and release of nucleotide, $\Omega_{10\to9}$, involve partially or primarily rotation *about* the major axis of the cross bridge. The Euler angles of the state transitions related to production of force, $\Omega_{11\to10}$, involve only the rotation of the major axis of the cross-bridge. The angular distributions for these Euler angles are discussed below.

(*H*) *Angular Distribution of Cross-Bridges in Rigor, MgADP, Isometric Contraction, and Relaxation at Low Ionic Strength.* Figure 4 shows the polar angular distribution, $n(\beta)$, of the cross-bridge principal hydrodynamic frame in rigor, isometric contraction, and relaxation at low ionic strength. The rigor distribution peaks at 87°. The low ionic strength relax condition has a distribution similar to that of rigor and a peak at 90°. The polar angular distribution of the cross-bridge in the presence of MgADP is identical to that in rigor, as suggested previously (Ajtai et al., 1992b). Activation of the fiber causes a large change in the cross-bridge distribution. The active isometric fiber polar angular distribution is comparatively broad but has a peak at 61°. The Euler angles indicate that if the transition of cross-bridges from active to the rigor state is characterized as a single rotation, then this transition causes a rotation of the major axis of the cross-bridge through 35°. The polar distributions shown in Figure 4 are identical for equivalent solutions A and B.

Figure 5 shows the torsinal angular distribution, $m(\gamma)$, for cross-bridges in rigor, MgADP, and isometric contraction. The rigor and MgADP distributions are nearly identical in shape but are shifted 10° relative to each other. The rigor

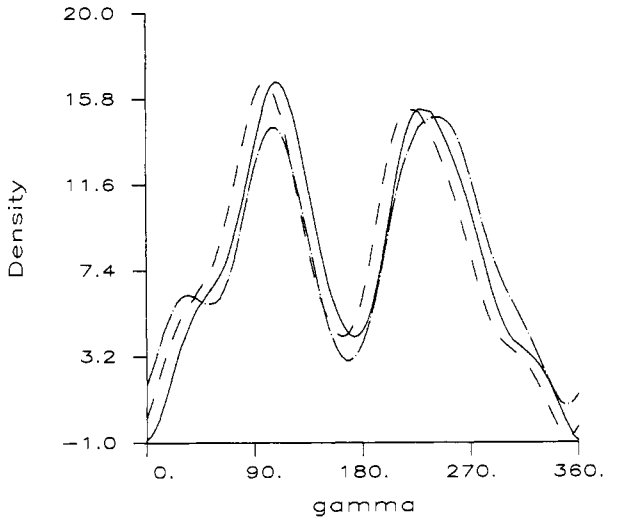

FIGURE 5: Torsional angular distribution, $m(\gamma)$, for muscle fiber cross-bridges in rigor (- - -), in the presence of MgADP (—), and in isometric contraction (– • –).

distribution peaks at 98° while the MgADP distribution peaks at 108°. All curves are bimodal with the high γ peak lying ~120° from the low γ peak. The peaks of the active isometric curve lie near the rigor and MgADP peaks but the distribution of cross-bridges between the low and high γ values is quite different. It seems evident that changes in the torsional distribution accompany cross-bridge activation but the interpretation of these changes is less obvious than in the case of the polar distribution changes.

While the polar angular distributions for rigor and MgADP are identical, the torsion angle distribution shows distinctive shifts. The torsional degree of freedom is a primary or significant mode of movement for physiological state transitions involving the binding and release of nucleotides. The polar distribution for the active isometric state (Figure 4) distinguished it from all other states and indicates that the polar degree of freedom is the primary mode of movement for physiological state transitions involving force generation.

The torsional distributions in Figure 5 are altered by the transformation $\gamma \rightarrow \pi - \gamma$ when solution A (shown in Figure 5) is compared with solution B (not shown). We cannot choose one of these two possibilities as the correct one because, on the basis of the available data, we cannot fix the position of the two minor axes in the prolate ellipsoid we chose to represent S1.

DISCUSSION

The present study of myosin cross-bridge order in muscle fibers demonstrates three new technical features of the MPA method. First, we now recast the data from the specific spin and fluorescent probes of myosin in terms of the principal hydrodynamic frame of the cross-bridge. This allows us to follow the movement of the cross-bridge (idealized as a prolate ellipsoid) rather than the movement of a probe fixed reference frame. Second, the scope of the application with five probes of four physiological states gives sufficient constraints to solve for cross-bridge orientation without data from every probe in every physiological state. We solved for cross-bridge orientation in the four physiological states using spin-labeled S1 decorating fibers in rigor and in MgADP and fluorescent-labeled fibers in all four physiological states and avoided the use of spin-labeled fibers with their associated artifacts. Third, the constraints of the MPA method that accompany the large data set collected from the fluorescent probes of the fiber, i.e., the 15 polarization ratios defined in eqs 1–5, break all of the

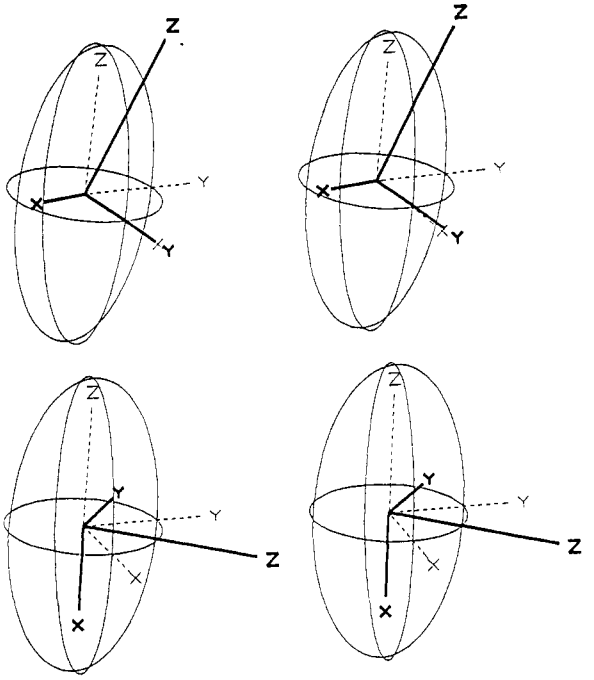

FIGURE 6: Stereoview of the orientation of [^{15}N,^{2}H]MTSL (top) and [^{15}N,^{2}H]IPSL (bottom) on S1 for Euler angles of solution A given in Table 1. The dashed coordinate axis represents the principal hydrodynamic frame of S1 and the solid coordinate axis the principal magnetic frame of the spin probe.

fundamental symmetries inherent in the probe detection techniques. We find that only one unresolved ambiguity remains in the estimate of cross-bridge orientation and order in the four physiological states studied. This ambiguity is introduced by our assumption of a prolate ellipsoid shape for the cross-bridge and manifests itself as the equivalence of solutions A and B mentioned in section H of Results.

The new technical advantages of the MPA of myosin cross-bridge orientation in muscle fibers inform us of previously unknown characteristics of the probe-modified protein and of the mechanism of muscle contraction. We investigated the relative orientation of the probes with the principal hydrodynamic frame of S1. Combining EPR data of spin-labeled S1 freely tumbling in solution measured at X- and Q-band microwave frequencies, we determined the rotational diffusion constants of S1, the extent of local probe movement, and two of the three Euler angles relating the probe principal magnetic frame with the principal hydrodynamic frame of S1. The observed diffusion constants imply that S1 has a major/minor axis ratio, $p \approx 3.8$, in agreement with previous findings of fluorescent-labeled S1, when labels are localized at SH1 (Mendelson et al., 1973; Van der Heide, 1992). We use movement within a cone to characterize the extent of local probe movement and find that the spin probes exhibit a 9–10° cone angle for local movement. This is larger than 15IA and about equal to 5′IATR on SH1 (see below). It is noteworthy that we found that the orientation of the two spin labels within S1 are radically different, as shown in Figure 6, despite the fact that they have similar probe angular distributions on decorated fibers in rigor and in MgADP (Ajtai et al., 1990, 1992b). While the z-axis of its principal magnetic frame of [^{15}N,^{2}H]MTSL-S1 points within 20° of the major axis of S1, the equivalent axis of [^{15}N,^{2}H]IPSL points along a minor axis of S1. The relaxation time for S1 major axis tumbling is known to be ~200 ns (Mendelson et al., 1973), implying that the relaxation time for S1 minor axis tumbling (and ([^{15}N,^{2}H]IPSL-S1) is ~70 ns [using the equations of Perrin as summarized in Cantor and Schimmel (1980) and $p = 3.8$].

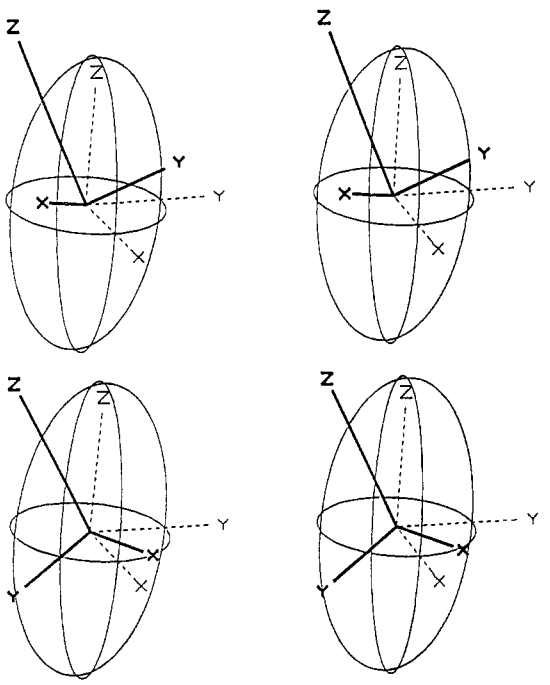

FIGURE 7: Stereoview of the orientation of 15IA (top) at λ_{ex} = 410 nm and 5'IATR (bottom) on S1 for Euler angles of solution A given in Table 1. The dotted coordinate axis represents the principal hydrodynamic frame of S1. The emission dipole lies along the solid line z-axis, and the excitation dipole lies in the solid line x–z plane at 22.3° (15IA) and 18.7° (5'IATR) from the z-axis.

Previously, we reported that the change in the hyperfine splitting extrema from immobilized to freely tumbling IPSL-S1 was larger than that from MTSL-S1 (Ajtai et al., 1990). This is indicative of a more rapidly tumbling spin probe in IPSL-S1 than in MTSL-S1 (Freed, 1976), in agreement with the more quantitative results presented here.

We measured, as have others before us, the TRFAD from 15IA- and 5'-IATR-labeled S1 (Mendelson et al., 1973; Ajtai et al., 1992a). TRFAD from 15IA-S1 indicates the rapidity of rotational movement of S1, some features of the relationship of the probe transition dipoles to the S1 principal hydrodynamic frame, and the cone angle for local probe movement. We observed a single ~200-nm relaxation due to S1 rotation with 15IA oriented with transition dipoles making an angle of <40° with the major axis of S1, in agreement with previous work (Mendelson et al., 1973). We also estimated the cone angle for local probe movement to be <2°. The TRFAD from 5'IATR-S1 gave no new information since the probe lifetime is too short to sense protein movement. Previously, we estimated a cone angle for local probe movement of 5'IATR-S1 to be ~10° (Ajtai et al., 1992a). The majority of the information relating the orientation of the fluorescence transition dipoles to the principal hydrodynamic frame of the S1 comes from the MPA of the combined data sets from labeled muscle fibers. This information is summarized in Figure 7, showing the stereoview of the probe transition dipoles in the principal hydrodynamic frame of S1.

The main results of the MPA are the surmised angular distributions of the S1 principal hydrodynamic frame in the four physiological states considered; see Figures 4 and 5. These results give us new information about cross-bridge orientation during the cross-bridge cycle in muscle contraction. The orientation of the cross-bridge major axis in rigor is usually assigned an angle in the 45–65° range with the fiber axis. This range of angles is suggested by electron microscopic (EM) images (Reedy et al., 1965; Reedy, 1968; Milligan & Flicker, 1987), the modeling of X-ray diffraction patterns (Holmes et al., 1980), and birefringence measurements of fibers in rigor (Peckham & Irving, 1989). Other EM work has indicated two orientations in rigor cross-bridges from insect flight muscle (Taylor et al., 1984). Alternatively, EM images from insect flight muscles prepared by the quick-freeze, deep-etch replica technique suggested that the mean rigor cross-bridge angle is nearer to 90° and that acutely angled rigor cross-bridges (observed with EM) is an artifact of the sample fixing procedure (Heuser & Cooke, 1984). EM images of strained cross-bridges indicate a wide range of possible orientations for the rigor cross-bridge (Trombitás et al., 1986). Our findings agree with a near perpendicular orientation of the rigor cross-bridge relative to actin; however, we equate cross-bridge orientation with the principal hydrodynamic frame of S1. The relationship between the principal frame of S1 and the shape of the EM image is very qualitative, and it seems quite possible that they could be 20–30° apart.

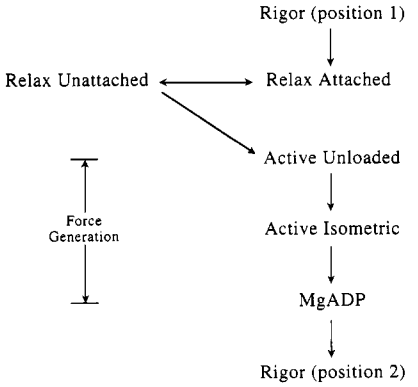

FIGURE 8: Contraction cycle of the myosin cross-bridge showing seven states of myosin S1. The active unloaded state was not observed experimentally but was surmised from the polar angular distribution of the active isometric state. The most likely orientation of the cross-bridge in these states is indicated in the space-filling models of Figure 9.

Figure 8 shows a flow diagram connecting six observable physiological states of the muscle fiber. Figure 9 shows space-filling models of acto-S1 for the most likely S1 orientations in the actin-bound states of Figure 8. In our description of the cross-bridge cycle (Figure 8), a rigor cross-bridge at position 1 binds MgATP and rotates with both polar and torsinal degrees of freedom to the low ionic strength relaxed (weakly bound) state. The weakly bound cross-bridge detaches and rebinds weakly to actin (Brenner et al., 1982) or goes on to the strong binding state, the active unloaded state. The weakly bound state is not the immediate precursor to the active unloaded state. A large polar rotation generates force (or does work on actin or both) and releases phosphate from S1. The active cross-bridge ends in the MgADP state. Release of MgADP is accompanied by a torsional rotation of S1 returning the cross-bridge to the rigor state at position 2 on actin. Only the orientation of the active unloaded state, shown in Figures 8 and 9, was not observed experimentally. We computed the most likely position of the active unloaded cross-bridge by estimating the largest value of the cross-bridge polar angle that is within the half-width of the polar angular distribution of the active isometric state shown in Figure 5. We assume that the transition from the active unloaded to active isometric state involves only a polar angular change.

Our analysis shows that the weakly bound cross-bridge has an orientation relative to actin rather closer to that of rigor than that of the active unloaded state, in agreement with previous work (Pollard et al., 1993). It seems that the weakly bound cross-bridge must detach from actin before interring the strongly bound state. Our analysis also shows that the

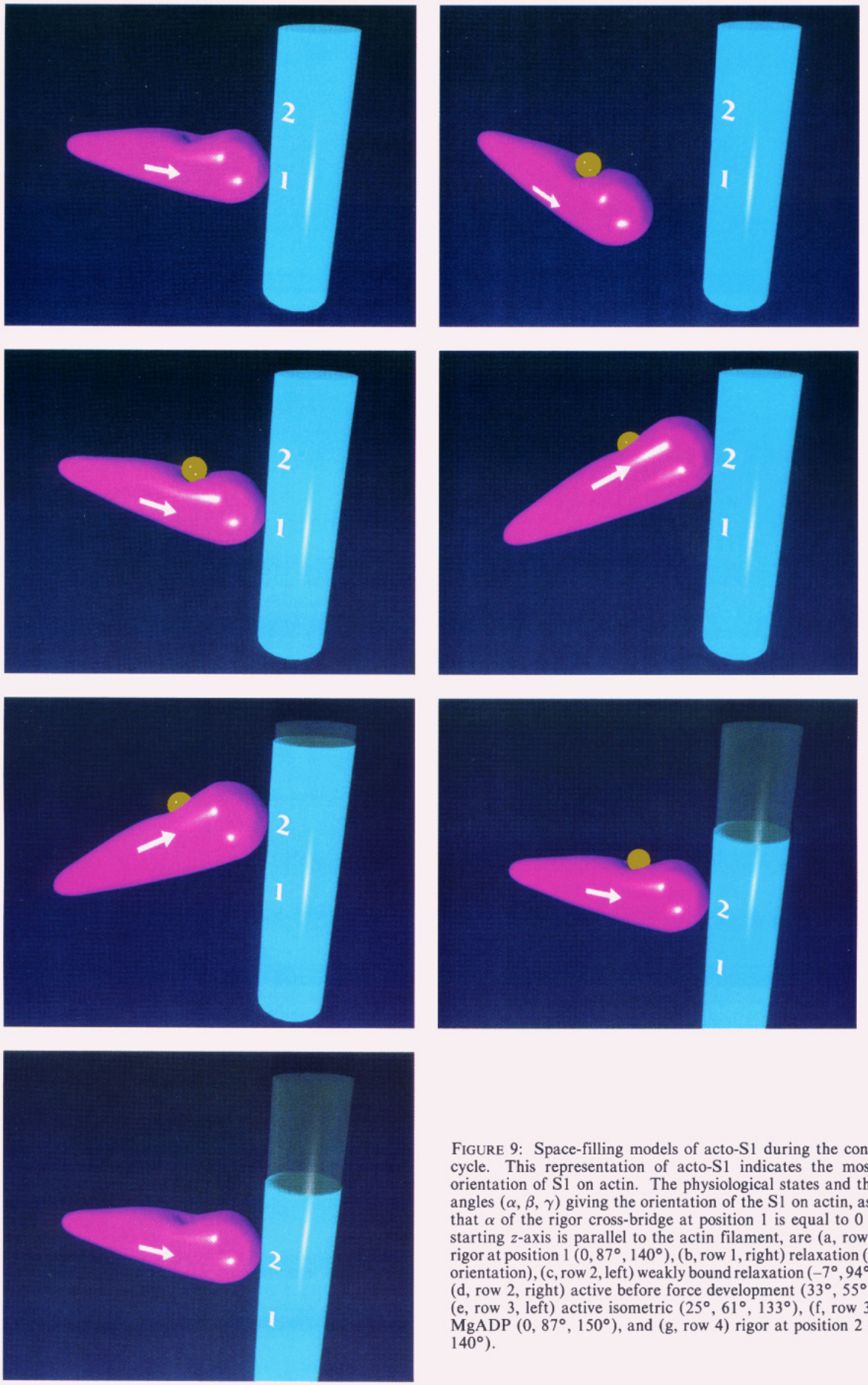

FIGURE 9: Space-filling models of acto-S1 during the contraction cycle. This representation of acto-S1 indicates the most likely orientation of S1 on actin. The physiological states and the Euler angles (α, β, γ) giving the orientation of the S1 on actin, assuming that α of the rigor cross-bridge at position 1 is equal to 0 and the starting z-axis is parallel to the actin filament, are (a, row 1, left) rigor at position 1 (0, 87°, 140°), (b, row 1, right) relaxation (random orientation), (c, row 2, left) weakly bound relaxation (–7°, 94°, 145°), (d, row 2, right) active before force development (33°, 55°, 129°), (e, row 3, left) active isometric (25°, 61°, 133°), (f, row 3, right) MgADP (0, 87°, 150°), and (g, row 4) rigor at position 2 (0, 87°, 140°).

rotation of S1 is partitioned into separate degrees of freedom depending on function. The binding and release of nucleotides is associated with the torsional rotation of S1. Both the rigor to low ionic strength relaxed transition ($\Omega_{9\rightarrow12}$) and the MgADP release step ($\Omega_{10\rightarrow9}$) cause the torsional rotation of S1. On the other hand, the observed force-producing state transition, active isometric contraction to MgADP ($\Omega_{11\rightarrow10}$), is a large and solely major axis rotation of the S1. Clearly, cross-bridge function is related to the rotational degree of freedom.

Recent observations concerning cross-bridge shape (Rayment et al., 1993a; Wakabayashi et al., 1992; Highsmith & Eden, 1990; Cheung et al., 1991) and action (Rayment et al., 1993b; Hirose et al., 1993; Pollard et al., 1993) during contraction favor the view that the cross-bridge undergoes an elaborate internal structural change during the ATPase cycle. Summarized simply, these observations suggest that only a part of the S1 reorients relative to actin during contraction. Assuming that these observations are correctly interpreted, then our present findings imply that the SH1 region of S1 is on a rigid portion of the cross-bridge that rotates on actin with the path and extent described herein.

The summary of our findings shown in Figures 8 and 9, indicating cross-bridge orientation through the active cycle, indicates the path and extent of cross-bridge orientation change during contraction. For probes of SH1 on S1 the cross-bridge rotates as a rigid body through a large angle while attached to actin as the cross-bridge progresses through its cycle. The power stroke evokes a major axis rotation of S1 that exceeds 35° while enzymatic functions of the cross-bridge (binding and release of nucleotides) evoke smaller torsional rotations of S1. All of the static states are orientationally distinct, and this distinctiveness manifests itself to varying degrees through all of the spin and fluorescent probes of SH1 in a predictable way described by the MPA.

ACKNOWLEDGMENT

We thank Jan M. Case and David T. Smyrk of the Mayo Foundation for creating and animating the space-filling model of the active cross-bridge cycle and P. J. K. Ilich, also of Mayo, for drawing the stereoviews of the probe orientations in the prolate ellipsoid. The animated space-filling model of actomyosin in the active cycle is available on video tape from the authors.

REFERENCES

Ajtai, K., & Burghardt, T. P. (1989) *Biochemistry 28*, 2204–2210.

Ajtai, K., Póto, L., & Burghardt, T. P. (1990) *Biochemistry 29*, 7733–7741.

Ajtai, K., Ilich, P. J. K., Ringler, A., Sedarous, S. S., Toft, D. J., & Burghardt, T. P. (1992a) *Biochemistry 31*, 12431–12440.

Ajtai, K., Ringler, A., & Burghardt, T. P. (1992b) *Biochemistry 31*, 207–217.

Borejdo, J., & Putnam, S. (1977) *Biochim. Biophys. Acta 459*, 578–595.

Borejdo, J., Putnam, S., & Morales, M. F. (1979) *Proc. Natl. Acad. Sci. U.S.A. 76*, 6346–6350.

Borejdo, J., Assulin, O., Ando, T., & Putnam, S. (1982) *J. Mol. Biol. 158*, 391–414.

Brenner, B. (1990) in *Molecular Mechanisms in Muscular Contraction* (Squire, J. M., Ed.) pp 77–149, Macmillan, London.

Brenner, B., Schoenberg, M., Chalovich, J. M., Green, L. E., & Eisenberg, E. (1982) *Proc. Natl. Acad. Sci. U.S.A. 79*, 7288–7291.

Burghardt, T. P., & Ajtai, K. (1992) *Biochemistry 31*, 200–206.

Burghardt, T. P., & Ajtai, K. (1994) *Biochemistry* (preceding paper in this issue).

Burghardt, T. P., Ando, T., & Borejdo, J. (1983) *Proc. Natl. Acad. Sci. U.S.A. 80*, 7515–7519.

Burghardt, T. P., Tidswell, M. S., & Borejdo, J. (1984) *J. Muscle Res. Cell Motil. 5*, 657–663.

Cantor, C. R., & Schimmel, P. R. (1980) *Biophysical Chemistry*, Part II, pp 562–563, Freeman, New York.

Cheung, H. C., Gryczynski, I., Malak, H., Wiczk, W., Johnson, M. L., & Lakowicz, J. R. (1991) *Biophys. Chem. 40*, 1–17.

Cooke, R., Crowder, M. S., & Thomas, D. D. (1982) *Nature (London) 300*, 776–778.

Duke, J., Takashi, R., Ue, K., & Morales, M. F. (1976) *Proc. Natl. Acad. Sci. U.S.A. 73*, 302–306.

Freed, J. H. (1976) in *Spin Labeling: Theory and Applications* (Berliner, L. J., Ed.) pp 53–132, Academic Press, New York.

Graceffa, P., & Seidel, J. C. (1980) *Biochemistry 19*, 33–39.

Heuser, J. E., & Cooke, R. (1983) *J. Mol. Biol. 169*, 97–122.

Highsmith, S., & Eden, D. (1990) *Biochemistry 29*, 4087–4093.

Hirose, K., Lenart, T. D., Murray, J. M., Franzini-Armstrong, C., & Goldman, Y. E. (1993) *Biophys. J. 65*, 397–408.

Holmes, K. C., Tregear, R. T., & Barrington Leigh, J. (1980) *Proc. R. Soc. London B 207*, 13–33.

Huxley, H. E. (1969) *Science 164*, 1356–1366.

Huxley, A. F., & Simmons, R. M. (1971) *Nature (London) 233*, 533–538.

Irving, M., Lombardi, V., Piazzesi, G., & Ferenczi, M. A. (1992) *Nature (London) 357*, 156–158.

Lakowicz, J. R. (1983) *Principles of Fluorescence Spectroscopy*, pp 155–186, Plenum Press, New York.

Mendelson, R. A., Morales, M. F., & Botts, J. (1973) *Biochemistry 12*, 2250–2255.

Mendelson, R. A., Putnam, S., & Morales, M. F. (1975) *J. Supramol. Struct. 3*, 162–168.

Milligan, R. A., & Flicker, P. F. (1987) *J. Cell Biol. 105*, 29–39.

Nihei, T., Mendelson, R. A., & Botts, J. (1974) *Biophys. J. 14*, 236–242.

Peckham, M., & Irving, M. (1989) *J. Mol. Biol. 210*, 113–126.

Pollard, T. D., Bhandari, D., Maupin, P., Wachsstock, D., Weeds, A. G., & Zot, H. G. (1993) *Biophys. J. 64*, 454–471.

Rayment, I., Rypniewski, W. R., Schmidt-Bäse, K., Smith, R., Tomchick, D. R., Benning, M. M., Winkelman, D. A., Wesenberg, G., & Holden, H. M. (1993a) *Science 261*, 50–58.

Rayment, I., Holden, H. M., Whittaker, M., Yohn, C. B., Lorenz, M., Holmes, K. C., & Milligan, R. A. (1993b) *Science 261*, 58–65.

Reedy, M. K. (1968) *J. Mol. Biol. 31*, 155–176.

Reedy, M. K., Holmes, K. C., & Tregear, R. T. (1965) *Nature (London) 207*, 1276.

Tanner, J. W., Thomas, D. D., & Goldman, Y. E. (1992) *J. Mol. Biol. 223*, 185–203.

Taylor, K. A., Reedy, M. C., Córdova, L., & Reedy, M. K. (1984) *Nature (London) 310*, 285–291.

Tonomura, Y., Appel, P., & Morales, M. F. (1966) *Biochemistry 5*, 515–521.

Trombitás, K., Baatsen, P. H., & Pollack, G. H. (1986) *J. Ultrastruct. Mol. Struct. Res. 97*, 39–49.

Van der Heide, U. A., Gerritsen, H. C., Trayer, I. P., & Levine, Y. K. (1992) *SPIE Meeting on Time Resolved Laser Spectroscopy in Biochemistry III. SPIE 1640*, pp 681–689, Society of Photo-Optical Instrumentation Engineers, Bellingham, WA.

Wakabayashi, K., Tokunaga, M., Kohno, I., Sugimoto, Y., Hamanaka, T., Takezawa, Y., Wakabayashi, T., & Amemiya, Y. (1992) *Science 258*, 443–447.

Weeds, A., & Taylor, R. S. (1975) *Nature (London) 257*, 54–56.